Eur J Nucl Med (1989) 15:750–755

European Journal of Nuclear Medicine

Measurement of resolution and recovery in recent generation positron tomographs*

Terence Spinks[1], **Riccardo Guzzardi**[2], **and C. Riccardo Bellina**[2]

[1] MRC Cyclotron Unit, Hammersmith Hospital, London, UK
[2] CNR Institute of Clinical Physiology, Pisa, Italy

Abstract. In positron tomographic images, the ability to differentiate closely lying structures, the spillover of activity from a region into adjacent regions and the reduction in apparent isotope concentration in small structures are all dependent on spatial resolution. Resolution in the reconstructed image is affected by (i) detector size, (ii) the spatial sampling used (e.g. stationary, wobble), (iii) the amount of smoothing in the reconstruction process (or subsequent to reconstruction) and (iv) the image pixel size. Under ideal conditions, modern commercial tomographs can produce a reconstructed spatial resolution of 5 mm or less. However, this is rarely realisable in a clinical study due to the inadequacy of counting statistics and the amplification of statistical noise. In practice, a smoother filter has to be used. This paper presents a summary of practical measurements of spatial resolution, and the related count recovery, performed on recent generation positron tomographs. It is intended to contribute to the definition of methods of measuring these parameters which is part of an on going concerted action in positron tomography supported by the European Commision.

Key words: Spatial resolution – Count recovery – Positron tomography

Recently there have been moves, sponsored by the European Commision, towards standardisation of measurements made in positron tomography. Although this project is intended to encompass physical and clinical parameters, the former are by their nature more easy to define and are an essential basis for clinical studies. Consequently, the initial emphasis is on standardisation and comparison of the physical performance of different designs of positron scanner. The fundamental characteristic of a scanner is its spatial resolution. The purpose of this paper is to present a summary of practical measurements of spatial resolution, and the related image count recovery, performed on recent generation positron tomographs employing rings of bismuth germanate (BGO) detectors. This discussion is intended to contribute to the definition of methods of measuring these parameters.

Spatial resolution is a measure of the ability of a tomograph to separate two point (line) sources. The differentiation of closely lying structures, the spillover of activity from a region into adjacent regions and the reduction in apparent isotope concentration in small structures are all dependent on spatial resolution. It can be described in terms of the line spread function (LSF) in real space or its Fourier Transform, the modulation transfer function (MTF), in frequency space. In this paper the LSF is used as the function to describe spatial resolution.

The physical limit of resolution is termed the intrinsic resolution which is that for individual detector pairs in the system; this is determined by the detector width. Resolution in the reconstructed image is affected by a number of additional factors: (a) the sampling used (stationary, wobbled, linear, angular), (b) the amount of spatial smoothing (filtering) in the reconstruction process (or subsequent to reconstruction), (c) the fineness of the grid on which the image is displayed. Under ideal conditions, modern commercial tomographs can produce a reconstructed spatial resolution of 5 mm or less. However, this is rarely realisable in a clinical study due to the inadequacy of counting statistics and the amplification of statistical noise. In practice, a smoother filter has to be used and the reconstructed resolution is consequently lower.

Materials and methods

Description of tomographs. The tomographs consisted of (i) 8 rings (15 transaxial image planes) – tomograph A (Spinks et al. 1988a) and (ii) 2 rings (3 planes) – tomograph B (Spinks, Guzzardi and Bellina 1988b); in both cases ring diameters were 102 cm. The detector elements of tomograph A had dimensions 5.6 (transaxial width) × 13.5 (axial length) × 30 mm (radial depth). Those of scanner B were 5.6 × 30 × 30 mm respectively. Both scanners were operated with inter plane lead/tungsten septa giving axial detector apertures of 10.5 mm (A) and 26.5 mm (B). In the case of A, the septa were of radial length 17 cm and thickness tapering from 3 mm (detector end) to 1 mm. For B, the septum was also 17 cm long but tapered from 12 mm to 3 mm. The scatter fractions were 12% (A – lower threshold 350 keV) and 30% (B – lower threshold 250 keV).

Transaxial resolution. Line sources, of internal diameter about 1 mm, were inserted axially into cylinders of scattering material (water, polythene or plexiglass) covering the axial field of view (FOV). Measurements were made at different distances from the centre (separated by 6–10 cm) and covered the normally used transaxial FOV. For tomograph

* This article was presented at the 1st EEC workshop on accuracy determination in PET, January 19–20th. 1989 Pisa, Italy (COMAC-BME Concerted Project "Characterization and Standardization of PET Instrumentation")

Offprint requests to: T.J. Spinks, MRC Cyclotron Unit, Hammersmith Hospital, Ducane Rd., London W12 OHS, UK

A, measurements were performed with (i) ^{68}Ge ($t_{1/2}$ = 270 days) in steel needles and (ii) ^{18}F ($t_{1/2}$ = 110 min) in plastic tubing. For tomograph B, line sources consisted of (i) ^{68}Ge and ^{68}Ga ($t_{1/2}$ = 68 min) in steel and plastic tubing respectively and (ii) ^{13}N ($t_{1/2}$ = 10 min) in plastic tubing. The internal diameter (i.d.) of the steel needles was 1.2 mm and the outer diameter (o.d.) 2.0 mm. The i.d. and o.d. of the plastic tubing were 1.0 mm and 1.5 mm respectively. In most cases, the line source was placed along the central axis of a 20 cm diameter cylinder and the phantom moved to different radial positions. For tomograph B, the plastic tubing was threaded through axial holes at different radial positions in a plexiglass cylinger of diameter 300 mm to enable simultaneous measurement to be performed.

For both scanners, acquisitions were carried out on the ^{68}Ge needles using the detectors in both stationary and wobble sampling modes and reconstruction was performed with a ramp filter (Nyquist cut off). This was intended to give information on the best attainable resolution of the systems. For the plastic line sources, only stationary sampling was used since this was the acquisition mode in clinical studies; reconstruction was done with both ramp and Hanning windows (Nyquist cut off). Attenuation correction was carried out by measurement (using external ^{68}Ge/^{68}Ga ring sources) and/or calculation and the effects of not correcting for attenuation were also examined. In order to eliminate any image distortion, the counting rates were kept low but counting times were sufficient to minimise the effects of statistical variations.

Following reconstruction, horizontal (tangential) and vertical (radial) profiles (line spread functions – LSFs) were defined through the maximum of the line source image. Parameters of resolution were obtained by linear interpolation of the LSF. Reconstructions were performed with a pixel size of less than 0.8 mm. Some of the data for tomograph A were reconstructed with larger pixel sizes (up to 2 mm/pixel) to test the effect on measured values. Full width at half and tenth maximum (FWHM and FWTM) were measured as well as equivalent width (EW), defined by:

$$\mathrm{EW} = \frac{\sum C_i \times \mathrm{PW}}{C_m} \quad (1)$$

where $\sum C_i$ is the total counts in the LSF, C_m the maximum pixel value and PW the pixel width (mm). The limits used for EW were 5% of the peak value.

Axial resolution. For tomograph A, a ^{68}Ge steel needle source was placed at right angles to the tomographic axis (in air) and moved in 0.8 mm axial steps. The centre of the source coincided with (i) the centre of the transaxial FOV and (ii) radial distances of 10 and 20 cm from this. The total counts for the LORs parallel to the radial displacement of the needle were used to define the LSF and hence axial resolution (FWHM and FWTM).

For tomograph B, a glass rod of internal diameter 3 mm and length 30 mm, containing ^{68}Ga, was placed at right angles to the axis and covered all appropriate radial positions (0, 6, 12 and 18 cm from the FOV centre). Data were again acquired in 0.8 mm steps. Dead time and decay corrections were applied due to the relatively short half life of ^{68}Ga but these were small. At each position, an image was reconstructed and regions of interest (ROIs) of width 6 cm were defined on the image with centres at the radial positions given. The plots of ROI counts vs axial position were interpolated with a Gaussian fit to give FWHM and FWTM.

Recovery. Count recovery with object size was tested with different geometries in the two scanners. In tomograph A, a phantom simulating the heart with varying myocardial wall thickness was used. This consisted of 2 cylinders of diameters 90 and 60 mm fitted inside each other with their axes offset. The cross section of the cavity between them had a radial thickness varying from 3–30 mm. This cavity (myocardium) was filled with active solution (^{18}F) and the central cavity (chamber) with water and vice versa. The length of the phantom covered the axial FOV and was inserted into a phantom simulating the thorax (with bottles at each side to simulate arms). ROIs of diameter 6 mm were defined on the myocardial image around the circumference of a circle tracing the mid point (radially) of the myocardium. A large ROI (diameter 35 mm) was placed centrally on the chamber image. In each case average pixel counts were divided by average counts from samples measured in a well counter (cross calibrated with the tomograph) to give normalised image pixel counts.

A variant of this phantom was used for tomograph B. This had a myocardial wall thickness ranging from 2–33 mm (inner and outer cylinder diameters 70 and 105 mm). The phantom was inserted into a cylinder of 20 cm diameter containing water. In all cases, the heart phantoms were placed close to the centre of the transaxial FOV and measured attenuation was carried out. Images were reconstructed with ramp and Hanning filters. No sampling of the active solution was carried out for tomograph B.

A 2nd arrangement used in tomograph A consisted of a set of spheres and rods alternately placed within an elliptical cylinder of o.ds. 240 × 150 mm. The range of diameters was from 7–36 mm. The centres of the spheres were coplanar (transaxially). They were filled with ^{18}F solution and the surrounding volume with water or with activity concentrations ranging from 8.5%–35% of the spheres. The rods were substituted for the spheres in order to eliminate the effect of partial volume in the axial direction. ROIs of diameter 6 mm were defined centrally on the image of each sphere and rod and counts/pixel compared with mean counts/pixel from (i) ROIs (diameter 25 mm) placed at the same locations and (ii) a large elliptical ROI of diameters 160 × 100 mm surrounding the positions of the spheres/rods in the cylinder containing the uniform solution. In all cases samples were taken from each of the phantom structures and counted in the well counter.

Results

Transaxial resolution

Values of FWHM and FWTM for tomograph A (mean of all 15 planes) using the ^{68}Ge steel needle are shown in Tables 1a and 1b. The means of the eight direct and seven cross planes were not significantly different. As anticipated from geometrical considerations, tangential resolution is relatively constant over the FOV whereas radial resolution increases (by about 2 mm from 0–18 cm). For both acquisition modes there is, in general, a slightly decreasing trend in FWHM and FWTM from measured to calculated to no attenuation correction. The mean difference in FWHM

Table 1a. Tomograph A – wobble sampling/ramp filter steel needle sources. Mean of 15 planes – values in mm

Distance from FOV centre (cm)		Attenuation correction					
		Measured		Calculated		None	
		FWHM	FWTM	FWHM	FWTM	FWHM	FWTM
0	R	5.5	11.0	5.7	10.8	5.2	10.3
	T	5.6	11.2	5.6	11.5	5.2	10.5
10	R	5.8	11.5	6.0	11.7	5.8	11.1
	T	5.7	11.6	5.6	11.6	5.3	10.6
18	R	7.8	16.3	7.6	15.0	7.4	14.3
	T	6.2	12.1	5.8	12.0	5.5	11.0

R = radial; T = tangential

Energy threshold = 350 keV

Table 1b. Tomograph A – stationary sampling/ramp filter steel needle sources. Mean of 15 planes – values in mm

Distance from FOV centre (cm)		Attenuation correction					
		Measured		Calculated		None	
		FWHM	FWTM	FWHM	FWTM	FWHM	FWTM
0	R	6.5	11.6	6.0	11.7	5.3	11.4
	T	6.1	11.7	5.9	12.6	6.9	11.4
10	R	6.4	12.1	6.6	12.4	6.4	11.8
	T	6.3	12.6	6.3	12.2	6.0	11.2
18	R	8.2	16.2	8.0	15.6	7.6	14.9
	T	6.8	13.5	6.6	12.8	6.4	12.3

R = radial; T = tangential

Energy threshold = 350 keV

(over the whole FOV) between measured and no attenuation correction is 0.3 mm (stationary) and 0.4 mm (wobble). However, for stationary sampling, anomalous behavior is observed at the centre of the FOV. This could be due to the under sampling at the centre which is characteristic of ring systems. Indeed, the wobble sampling does not show this.

Corresponding data for tomograph B are given in Table 2 which shows the comparison between stationary and wobble sampling using calculated attenuation correction. This again shows some anomalous behaviour at the centre of the FOV for stationary sampling. Comparison of the data in Table 2 with the calculated attenuation values in Tables 1a and 1b (at 0, 10 and 18 cm respectively) shows a mean difference of less than 0.1 mm in FWHM and 0.3 mm in FWTM (both wobble and stationary sampling). Since detector width and sampling modes are the same for the two tomographs, this indicates that the effect of different energy thresholds is negligible.

Tables 3a and 3b (tomograph B) and Table 3c (tomograph A) give FWHM and FWTM values for line sources where positron range was not restricted and where measured attenuation correction and stationary sampling were applied. For tomograph B, the mean differences in FWHM between ^{13}N and ^{68}Ga were 0.5 mm (both ramp and Hanning), pooling data for radial, tangential and all positions in the FOV. The corresponding differences for FWTM were 1.8 mm (both filters). The mean differences in FWHM

Table 2. Tomograph B – calculated attenuation correction/ramp filter. Mean of 3 planes – values in mm

Distance from FOV centre (cm)		Stationary		Wobble	
		FWHM	FWTM	FWHM	FWTM
0	R	6.0	11.0	5.4	10.8
	T	6.6	12.0	5.6	11.1
6	R	6.2	12.1	5.6	11.1
	T	6.0	11.6	5.3	10.7
12	R	6.8	13.2	6.3	12.1
	T	6.1	11.5	5.6	11.0
18	R	8.1	16.5	7.7	15.2
	T	6.3	12.0	5.6	10.9

R = radial; T = tangential

Energy threshold = 250 keV

(comparing 0 cm and 10/12 cm from the FOV centre) between ^{18}F (tomograph A) and ^{13}N (tomograph B) were 0.2 mm (both filters). The corresponding FWTM differences were 0.8 mm (ramp) and 0.7 mm (Hanning). On average, the change of FWHM is roughly 0.5 mm/MeV (positron E_{max}).

The average value of FWHM for ^{18}F (ramp filter – Table 3c) is 0.3 mm less than that (at corresponding posi-

Table 3a. Tomograph B – stationary sampling/ramp/measured attenuation correction plastic line sources. Mean of all planes – values in mm

Distance from FOV centre (cm)		^{13}N		^{68}Ga	
		FWHM	FWTM	FWHM	FWTM
0	R	5.9	10.6	6.3	11.9
	T	5.9	11.0	6.2	12.0
6	R	6.1	11.6	6.7	14.2
	T	5.9	11.0	6.6	12.5
12	R	6.5	14.1	7.0	15.8
	T	6.4	13.1	7.1	15.9
18	R	8.6	19.5	–	–
	T	7.5	14.5	–	–

R = radial; T = tangential

Table 3b. Tomograph B – stationary sampling/Hanning/measured attenuation correction plastic line sources. Mean of all planes – values in mm

Distance from FOV centre (cm)		^{13}N		^{68}Ga	
		FWHM	FWTM	FWHM	FWTM
0	R	8.4	15.4	8.7	16.5
	T	8.5	15.5	8.9	18.0
6	R	8.3	15.7	9.0	17.4
	T	8.5	15.8	9.0	17.1
12	R	8.7	16.4	9.1	17.8
	T	9.1	17.4	9.6	20.1
18	R	9.8	20.1	–	–
	T	9.9	19.6	–	–

R = radial; T = tangential

Table 3c. Tomograph A – stationary sampling/measured attenuation correction plastic line source – ^{18}F. Mean of all planes – values in mm

Distance from FOV centre (cm)		Hanning		Ramp	
		FWHM	FWTM	FWHM	FWTM
0	R	8.4	15.2	5.8	11.5
	T	8.3	15.1	5.9	10.4
10	R	8.9	16.2	6.4	12.5
	T	8.5	15.4	6.0	11.4

R = radial; T = tangential

tions) for ^{68}Ge (Table 1b) and FWTM is 0.6 mm less. This suggests that the steel needle wall thickness was insufficient to stop all of the positrons from ^{68}Ge (E_{max} = 1.90 MeV). In fact, FWHM for the steel needles scanned in air, where activity distribution is obviously restricted to the needles' o.d., are very similar to the values for no attenuation correction (Tables 1a and 1b). The highest resolution attainable (for wobble sampling at the centre of the FOV) is 5.2 mm FWHM. Deconvolving the needle diameter (0.2 mm) from this gives a FWHM of 4.8 mm or about 0.9 of the detector width.

Pooling the data for each radionuclide, the ratios

Table 4. Tomograph B – stationary sampling. Plane 1 – values in mm

Distance from FOV centre (cm)		Equivalent widths (Eq. 1)			
		^{13}N		^{68}Ga	
		Ramp	Hanning	Ramp	Hanning
0	R	6.4	9.1	7.1	9.7
	T	6.3	8.9	7.0	9.9
6	R	6.4	8.9	7.3	9.8
	T	6.3	9.0	7.0	9.7
12	R	7.5	9.3	8.0	9.9
	T	7.1	9.9	8.3	11.1
18	R	9.8	10.8	–	–
	T	8.1	10.9	–	–

R = radial; T = tangential

Table 5a. Tomograph A – axial resolution – values in mm

Distance from FOV centre (cm)	Direct planes		Cross planes	
	FWHM	FWTM	FWHM	FWTM
0	6.6	13.4	5.9	12.2
10	7.0	13.1	6.9	13.7
20	7.6	13.1	11.4	17.2

Table 5b. Tomograph B – axial resolution – values in mm

Distance from FOV centre (cm)	Direct planes (mean)		Cross plane	
	FWHM	FWTM	FWHM	FWTM
0	15.4	28.1	14.2	26.0
6	15.2	27.8	14.6	26.6
12	15.8	28.9	16.5	29.9
18	16.8	30.8	19.9	36.3

FWTM/FWHM were 1.97 (^{68}Ge/^{68}Ga), 1.98 (^{13}N) and 1.90 (^{18}F) for the ramp filter and 1.97 (^{68}Ge/^{68}Ga), 1.90 (^{13}N) and 1.82 (^{18}F) for the Hanning filter.

The data of Tables 1–3 were obtained using an image pixel size $\leq$0.8mm. The data in Table 3c, as an example, were reconstructed with varying pixel size. The average of radial and tangential FWHM (at 0 cm) was 8.4 mm for both 0.25 and 0.50 mm/pixel and increased to 8.5 mm at 1.0 and 2.0 mm/pixel. Therefore the change in measured values is not very sensitive to change in pixel size over this range but it is suggested that pixel size be at most one tenth of the FWHM.

Equivalent widths (eq. 1) are given in Table 4 for the ^{13}N and ^{68}Ga data of Tables 3a and 3b. Taking the data for both tracers (all positions and orientations), the mean ratios of Hanning/ramp are similar for the 3 parameters: 1.36 $\pm$ 0.08 (FWHM), 1.31 $\pm$ 0.14 (FWTM) and 1.34 $\pm$ 0.08 (EW). The ratio of ^{68}Ga/^{13}N data for EW (1.10 $\pm$ 0.03) fell between those for FWHM (1.07 $\pm$ 0.03 and FWTM (1.13 $\pm$ 0.05).

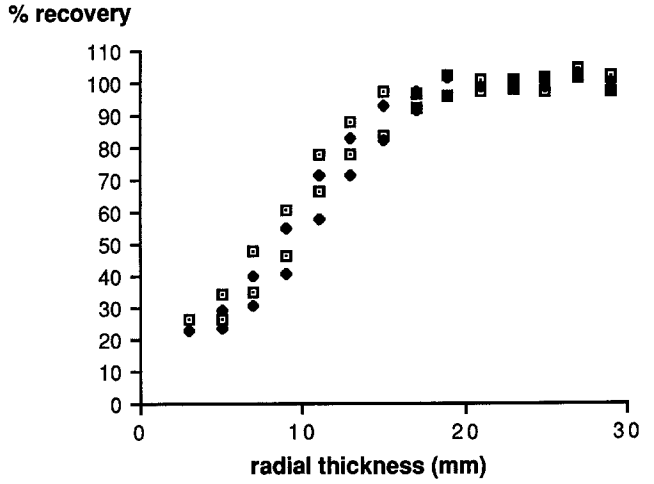

Fig. 1. Recovery curves for heart phantom (tomograph A – ^{18}F) with varable myocardial wall thickness, reconstructed with different filters. ▫ ramp filter; ◆ Hanning filter

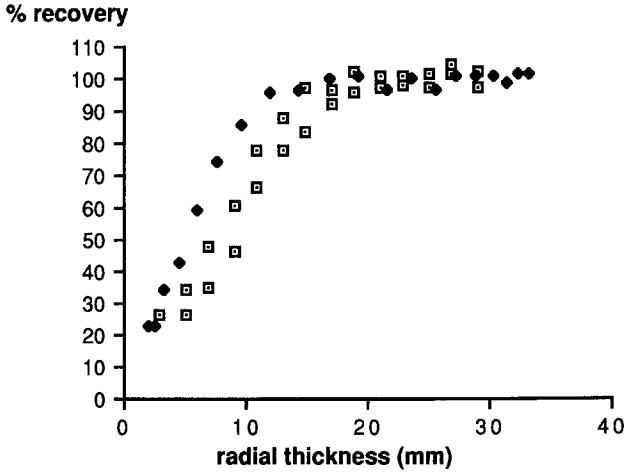

Fig. 2. Recovery curves for heart phantoms used in tomographs A (^{18}F) and B (^{68}Ga), reconstructed with the same filter. ▫ tomograph A; ◆ tomograph B

Axial resolution

Values of axial resolution (mean of direct and cross planes) are shown in Table 5a (tomograph A) and 5b (tomograph B). This shows, the expected relative stability in FWHM and FWTM over the FOV for direct planes and the increase with increasing radius for cross planes. The increase for cross planes between the centre and extreme position was 90% (tomograph A) and 40% (tomograph B). In both cases, the FWHM at the centre (direct planes) was close to 0.6 of the detector aperture; the FWTM was about 1.1 times the aperture.

Recovery

A comparison of count recovery curves, using the two reconstruction filters, for the myocardial phantom containing ^{18}F (tomograph A) is shown in Fig. 1. The x axis represents (radial) wall thickness. The ROI diameter was 6 mm (area 0.31 cm^2), corresponding to the FWHM for the ramp filter. The plateau is apparently reached for wall thicknesses greater than 25 mm. Taking this as 100%, recovery coefficients (RCs) at 15 mm and 10 mm are 91% and 63% (ramp) and 87% and 57% (Hanning), fitting the curves with a polynomial function. A comparison between these data and those for the phantom used in tomograph B are shown in Fig. 2 (ramp filter). The RCs for B at 15 and 10 mm are 97% and 87%, i.e. significantly higher than for A. Normalised pixel counts (tomograph A) for the plateau were 102% of the normalised central chamber pixel counts and 97% of normalised pixel counts from a 20 cm uniform cylinder.

Figure 3 shows a comparison between RC curves for the spheres and rods, placed in the elliptical cylinder filled with water. The Hanning filter was used (ROI diameter 6 mm). It should be noted that full (100%) recovery is defined by the normalised pixel counts in the uniformly filled cylinder. The mean counts/pixel for ROIs placed at the locations of the spheres/rods on the image of the uniform phantom was only 2% higher than that for the large ROI encompassing the smaller ROIs. At diameters of 15 and 10 mm RCs were 60% and 36% (spheres) and 70% and 46% (rods). Taking the plateau as the mean of the 2 largest

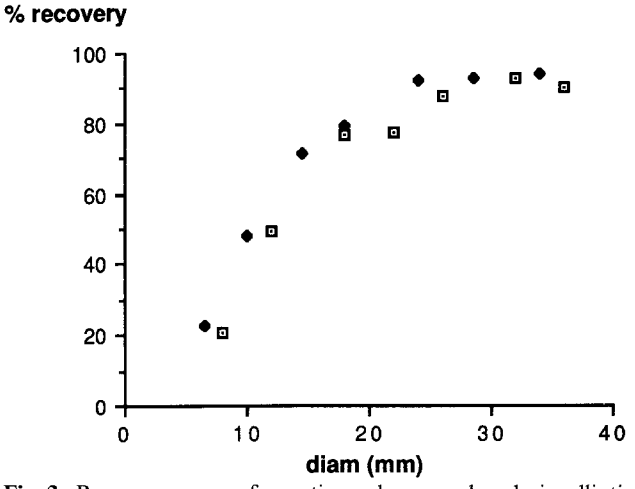

Fig. 3. Recovery curves for active spheres and rods in elliptical cylinder containing water (Hanning filter). ▫ sphere; ◆ rod

spheres/rods (≥25 mm), that for the spheres was 93% and that for the rods 95%. When a ROI diameter of 8 mm was used the reduction in recovery for the spheres at 15 mm was 6% and at 10 mm 9%. When this experiment was repeated with three different background activity concentrations surrounding the spheres, the plateau levels were 92%, 95% and 98% for background/sphere concentration ratios of 0.085, 0.17 and 0.35 respectively.

Discussion

Since the measurements performed on the two scanners in this study were not the same in all respects, a direct comparison of the two is not possible. The measurements were used rather in a complementary sense to provide an overall impression, from modern tomographs, of the factors to be taken into account in defining standard procedures. The tomographs were identical in their transaxial detector widths and spatial sampling modes. Resolution for the two was thus expected to be the same under the same conditions. On the other hand, they differed in the relative level of random and scatter events. Dead time was corrected for

in these tests but it was deliberately minimised and so not of importance. The influence of geometry, and hence scatter, on measurement of recovery is of much more importance.

Comparison of equivalent measurements (^{68}Ge steel needles/calculated attenuation correction) gave very similar results for the two tomographs, indicating negligible influence of energy threshold. The highest resolution achievable is close to 5 mm (or 0.9 times the detector width). The improvement in measured FWHM in going from stationary to wobble sampling is on average 0.6 mm.

The small dependence on the type of attenuation correction and uncertainties about positron range suggest that it is best to measure spatial resolution under in vivo conditions. In other words, line sources should be constructed of tissue/water equivalent material and attenuation correction should be performed as for a clinical study, whether it be measured or calculated. The activity in the source should have a diameter of no more than 1 mm. Information on the variation of spatial resolution over the range of radionuclides normally used could be usefully provided by ^{18}F (positron $E_{max}=0.64$ MeV) and ^{68}Ge ($E_{max}=$ 1.90 MeV). These two radionuclides are commonly available.

The conventional way to express resolution is by the FWHM and FWTM of the LSF. In this study, an alternative parameter, equivalent width (EW), is also suggested. This has the advantage of being a single number which also uses the whole of the LSF for its definition. Its sensitivity to positron range or filter is, as expected, greater than that of FWHM but less than FWTM. One disadvantage of EW is that it has not been commonly used in publications on positron tomography. A small technical problem is the definition of the limits between which the LSF should be integrated. The limits were restricted to 5% of the peak due to problems with negative undershoots using the ramp filter. However, when it was possible to go outside these limits there was little change in EW.

Values of axial resolution are not very sensitive to the method of measurement as long as there is adequate sampling. The sampling in these studies was 0.08 (A) and 0.03 (B) × detector aperture. The ratios between FWHM and FWTM and detector aperture were similar in the 2 cases indicating that a sampling of at least 0.1 × aperture is adequate. However, a convenient method of measurement is that employed for tomograph B where the source spanned all positions of the FOV simultaneously. This method had the additional advantage that measurements were made directly from the tomographic images and thus provided a more realistic assessment.

Measurement of recovery is obviously dependent on geometry, and hence scatter conditions, choice of ROI dimensions and definition of the 100% level. The plateau level for the myocardium of the heart phantom, which theoretically should have represented full recovery, had mean pixel counts of 102% relative to the chamber (which had twice the diameter) and 97% relative to a 20 cm diameter cylinder. Since no correction was made, these results are assumed to be an effect of scatter as is the difference between the curves in Fig. 2. The difference is not due to positron range (Spinks et al. 1988b). The apparent decrease in recovery below 100% for the spheres and rods of diameter more than 3 × FWHM is also considered to be due to the same effect. The change in recovery for these structures when the surrounding background activity was varied is also indicative of the influence of scatter. The definition of full recovery, depends on the method of calibration of the scanner. Normally, cross calibration is performed relative to a well counter which provides a constant geometrical reference (e.g. counts/s per g of solution from a phantom or blood from a patient). It is desirable to perform this cross calibration with a phantom simulating the geometry of the part of the body under study to minimise the effect of scatter.

References

Spinks TJ, Jones T, Gilardi MC, Heather JD (1988a) Physical performance of the latest generation of commercial positron scanner. IEEE Trans Nucl Sci 35:721–725

Spinks TJ, Guzzardi R, Bellina CR (1988b) Performance characteristics of a whole-body positron tomograph. J Nucl Med 29:1833–1841